Ring Genesis and the Related Heat Transport. Part II: A Model Comparison

SYBREN S. DRIJFHOUT

Royal Netherlands Meteorological Institute, De Bilt, the Netherlands

(Manuscript received 8 March 1991, in final form 22 July 1991)

ABSTRACT

Various ocean circulation models have been compared with respect to their performance in the genesis of rings and the subsequent heat transport. Emphasis has been placed on the role of the spurious diapycnal fluxes of heat and momentum in Cartesian models, arising when the horizontal dissipation mixes through sloping isopycnals.

Quasigeostrophic, isopycnal coordinate, and Cartesian primitive equation models in a two-layer periodic channel domain have been used to simulate the process of eddy detachment from an eastward-flowing jet. This jet is modeled after the Gulf Stream east of Cape Hatteras. On this jet a small sinusoidal disturbance is superimposed, which, through the release of available potential energy, grows until it ultimately has developed into ringlike eddies.

Simulations with the Cartesian primitive equation model appear to suffer from spurious diapycnal mixing of both heat and momentum. This retards the process of Rossby wave breaking and prolongs the growth of the meander, thus causing a doubled heat transport at 10-km resolution, compared to a 5-km resolution experiment. The isopycnic model does not show this degree of overshoot in heat transport. In general, the Cartesian model is much more sensitive to both resolution and closure formulation than the isopycnic model.

The quasigeostrophic model does not simulate the small-scale processes of Rossby wave steepening and breaking correctly. However, as a consequence the diapycnal mixing of heat and momentum hardly affects these processes. For this reason, the quasigeostrophic model does not show an overshoot in heat transport.

1. Introduction

It has now been well established that the ocean circulation is influenced by mesoscale eddies that are abundant almost everywhere (see, e.g., Robinson 1983). Their influence on the general circulation is mainly due to their role as transferring agents of material properties, such as heat, salt, and potential vorticity, and in the horizontal and vertical transport of momentum by means of Reynold stresses (Robinson et al. 1977; Holland and Rhines 1980; Holland et al. 1984; Böning and Cox 1988).

For a long time (Iselin 1939; Montgomery 1940) it has been believed that mixing of material properties by eddies mainly occurs along isopycnal surfaces. In general this is true, since below the surface mixed-layer water parcels approximately conserve their density, i.e., they move along isopycnals. However, when the formation of rings (elliptic eddies with specific water mass properties, separated from their surroundings by a front) is considered, we observe the breaking of isopycnal surfaces through the curling and closing of potential vorticity contours. As a result, the rings transfer properties of their parent water mass to a different water mass (Robinson et al. 1974, 1988; Drijfhout 1990).

Whether or not this diapycnal flux will be compensated by an eddy-induced mean circulation (Semtner and Mintz 1977; Cox 1985; Bryan 1986), which means that in a statistical sense eddies still act as isopycnal diffusers, is yet unclear.

As the observational database is still too sparse to deduce the reliable second-order statistics to settle questions about the physical processes that govern eddy mixing, experiments with high-resolution ocean models are very useful to gain insight. However, the simulated physics may depend heavily on model features such as the ratio of explicit to implicit diffusivity and viscosity, the model resolution, the turbulence closure formulation, etc. Also, the basic model formulation may be of importance: for example, whether quasigeostrophic or primitive equations are used and the choice of the vertical coordinate; that is, whether the equations are solved on horizontal or on isopycnal surfaces.

Most recent sensitivity studies concerning parameterization and model formulation have focused mainly on the sensitivity of the thermohaline circulation to the vertical diffusivity (e.g., Bryan 1987; Cummins et al. 1990) and on the role of the model formulation in the simulation of an eddy-resolving flow field (e.g., Bleck and Boudra 1986; Spall and Robinson 1990).

Corresponding author address: Mr. Sybren S. Drijfhout, Royal Netherlands Meteorological Institute, P.O. Box 201, 3730 AE De Bilt, The Netherlands.

In the present study we have tested to what extent model differences influence the formation of rings along ocean fronts and their subsequent heat transport. We have studied the effects of resolution, closure formulation, and model formulation. We have considered three different types of models: a quasigeostrophic model, an isopycnic primitive equation model, and a Cartesian primitive equation model. In this study, the same experimental setup is used for the simulation of rings in an unstable oceanic jet as described in Drijfhout (1990).

Emphasis will be placed on the role of two spurious effects that occur in Cartesian models when isopycnals are inclined with respect to the horizontal: 1) The spurious diapycnal mixing of density and momentum resulting from both the lateral mixing operating on horizontal surfaces and from the truncation error in the horizontal advection schemes. 2) The spurious generation of potential vorticity that results from a non-potential-vorticity-conserving advection scheme.

This paper is organized as follows. In section 2 we outline the numerical models used. In section 3 the effect of resolution in the Cartesian primitive equation model is demonstrated and analyzed. In section 4 we explore the sensitivity to the closure formulation. Section 5 consists of a comparison between a quasigeostrophic, an isopycnic, and a Cartesian primitive equation model. In section 6 we discuss the main results and present our conclusions.

2. The numerical models

We have used three models in this study: a Cartesian primitive equation model, a quasigeostrophic model, and an isopycnic primitive equation model. The Cartesian primitive equation model follows the principles outlined by Bryan (1969). The usual simplifications—in the form of the hydrostatic, the Boussinesq, and the β-plane approximation, the incompressibility condition, and a linearized equation of state—have been applied. Instead of Laplacian friction, the more scale-selective biharmonic friction is used, see Holland (1978) for a discussion. The governing equations of the model are

$$u_t + \mathbf{u}\cdot\nabla u + wu_z - fv = -p_x/\rho_0 - B_M\nabla^4 u \quad (2.1)$$

$$v_t + \mathbf{u}\cdot\nabla v + wv_z + fu = -p_y/\rho_0 - B_M\nabla^4 v \quad (2.2)$$

$$T_t + \mathbf{u}\cdot\nabla T + wT_z = -B_T\nabla^4 T. \quad (2.3)$$

The equation of state is linearized around a reference temperature: i.e.,

$$\rho = \rho_0[1 - a(T - T_0)] \quad (2.4)$$

giving a static pressure

$$p_z = -\rho g. \quad (2.5)$$

The continuity equation reads

$$\nabla\cdot\mathbf{u} + w_z = 0. \quad (2.6)$$

In these equations $\mathbf{u} = (u, v)$ is the horizontal velocity, w, p, T, and ρ represent vertical velocity, pressure, temperature, and density. The ∇ operator applies to horizontal coordinates only. The numerical formulation guarantees conservation of momentum, mass, temperature, and energy, apart from dissipation terms.

The governing equations are solved within a domain of 320 km $\times$ 1000 km with a flat bottom at 4200-m depth. The boundary conditions are periodic in the east–west direction. At the closed boundaries, we use a no-slip condition and there is no heat and mass flux out of the domain. No external forcing is used. The gridpoint arrangement is chosen as the Arakawa C grid (see Arakawa and Lamb 1977). For further details see Drijfhout (1990).

The quasigeostrophic model is described by Ikeda (1981) and Ikeda and Apel (1981). The model equation is

$$q_t + \mathbf{u}\cdot\nabla q = -B_M\nabla^4\xi - B_T\nabla^4\eta, \quad (2.7)$$

where

$$q = \nabla^2\psi + f + F_i(\psi_2 - \psi_1)S_F \quad (2.8)$$

represents the potential vorticity and $F_i = \rho_0 f_0^2/(\Delta\rho g H_i)$, a parameter related to the internal Rossby radius;

$$F_1 + F_2 = R_D^{-2}; \quad F_1 \to R_D^{-2}, \quad \text{when} \quad H_2 \to \infty.$$

Here ψ_i is the streamfunction, $\xi = \nabla^2\psi$ is the relative vorticity, and $\eta = F_i(\psi_2 - \psi_1)$ is the thermal vorticity. The subscript i denotes the level; H_i is the layer depth. This equation is solved with a second-order upstream differencing scheme, after which ψ is determined by relaxation.

The isopycnic model is described by Bleck and Boudra (1986):

$$u_t + \mathbf{u}\cdot\nabla u - fv = -M_x - B_M\nabla^4 u \quad (2.9)$$

$$v_t + \mathbf{u}\cdot\nabla v + fu = -M_y - B_M\nabla^4 v. \quad (2.10)$$

The hydrostatic equation reads

$$M_s = p\frac{\partial}{\partial s}(1/\rho) \quad (2.11)$$

and the continuity equation:

$$\frac{\partial}{\partial t}(\partial p/\partial s) + \nabla\cdot\mathbf{U} = 0. \quad (2.12)$$

In these equations M is the Montgomery potential, $\mathbf{U}$ is the horizontal mass transport, and s is the vertical coordinate of the isopycnic model. The finite difference form of the momentum equations is cast in a potential vorticity conserving form (see Bleck and Boudra 1981). Equation (2.12) is solved with a flux corrected transport (FCT) algorithm, (Boris and Book 1973; Zalesak 1979). The FCT algorithm prevents overshooting caused by the normally used second-order schemes and

makes the occurrence of layers with negative thickness values impossible.

The initial state used in the experiments consists of an eastward-flowing jet between $-L/2 < y < L/2$. This jet results from a density and dynamic height step across the front modeled by a half-sine between $-L/2 < y < L/2$. As an initial perturbation, a small sinusoidal disturbance with a wavelength equal to the length of the basin is superimposed. The resulting form for the initial profile is

$$p(z) = C(z)[\sin(\pi y/L) + 0.1 \cos(\pi y/L) \sin(2\pi x/D)], \quad (2.13)$$

where D is the length of the domain and $C(z)$ determines the strength and the vertical structure of the jet. Initial velocities are computed by requiring geostrophic balance. In the isopycnic model, this initial state is prescribed for $M(z)$.

The structure of the jet is modeled after the Gulf Stream according to Flierl (1975). For a two-layer model this results in the following set of parameters:

$$f_0 = 8.7 \times 10^{-5}\ \text{s}^{-1},\ \beta = 1.8 \times 10^{-11}\ \text{m}^{-1}\ \text{s}^{-1},$$

$$H_1 = 760\ \text{m},$$

$$H_2 = 3440\ \text{m},\ U_1 = 90.3\ \text{cm s}^{-1},\ U_2 = 19.7\ \text{cm s}^{-1},$$

$$L_e = 85.8\ \text{km},\ R_d = 29.2\ \text{km},\ g' = 1.02\ \text{cm s}^{-2},$$

where R_d is the Rossby radius of deformation and $g' = g\rho/\rho_0$. For a further discussion of the initial state and more details about the various model parameters, refer to Drijfhout (1990).

The equations for the various components of the energy budget can be derived from Eqs. (2.1)–(2.12). They are described in the Appendix. To make comparison between the different models possible, an equivalent temperature is formulated to equate the pressure difference between the upper and lower level (layer). Then the initial available potential energy can be made equal for all three models (on a given coordinate surface).

3. Model resolution

a. *Viscosity and model truncation*

We define the viscosity and diffusivity in the numerical model as the amount of mixing of momentum, density, accomplished by the resolved eddy field (implicit friction and diffusion) plus a contribution of the unresolved eddy field, parameterized through a closure formulation (explicit or artificial friction and diffusion). It is obvious that changing the horizontal resolution affects the viscosity and diffusivity of the model. It necessitates a change in the explicit friction and diffusion parameters, as they are related to the model truncation. In a way, the explicit friction and diffusion parameters control the spectral energy and enstrophy flux at the short-wave end of the spectrum and, consequently, the amplitude of the smallest resolved scales. Therefore, the magnitude of these parameters should be adapted to the resolution, that is, the amount of truncation.

The total amount of dissipation of energy and enstrophy for two-dimensional flow can be written as (Batchelor 1953)

$$\frac{\partial}{\partial t}\int Edk = -24\nu \int k^4 Edk, \quad (3.1)$$

$$\frac{\partial}{\partial t}\int Sdk = -24\nu \int k^4 Sdk = -24\nu \int k^6 Edk. \quad (3.2)$$

In these equations E is the energy and S is the enstrophy, ν is a dissipation parameter; we have assumed biharmonic friction. If the resolution is increased and consequently the maximum value of k at which we truncate the model, from Eqs. (3.1) and (3.2) the total amount of enstrophy dissipation increases more than the energy dissipation. By changing ν we cannot make both the energy and enstrophy dissipation independent of the truncation.

Assume that large-scale two-dimensional turbulence is at first order a good model for the processes being studied. According to Charney (1971), results from two-dimensional turbulence can be generalized to quasigeostrophic three-dimensional flows. In such (inviscid) flows in statistical equilibrium there are no spectral energy fluxes at scales smaller than the Rossby radius of deformation. However, there is an enstrophy cascade toward smaller scales (e.g., Monin and Ozmidov 1985).

Within a numerical model, the enstrophy cascade is affected by the truncation. As the spectral enstrophy flux cannot pass the smallest resolved scale, enstrophy will increase at high wavenumbers relative to the lower wavenumbers. This process prevents the model from reaching the equilibrium spectrum, and also an energy cascade toward the smallest scales will be induced. To balance the enstrophy and energy increase at high wavenumbers, artificial dissipation is needed. Formally, the magnitude should be

$$-24\nu(k_{\max}) \int_{k_0}^{k_{\max}} k^4 Edk = -\Delta F_E, \quad (3.3)$$

$$-24\nu(k_{\max}) \int_{k_0}^{k_{\max}} k^4 Sdk = -\Delta F_S, \quad (3.4)$$

where k_0 is the long-wave end of a viscous subrange, $k_{\max}$ is the wavenumber at which the model is truncated, and ΔF is the flux difference between the long- and short-wave end of the viscous subrange. In theory, the spectral enstrophy flux is a constant, say F_S^*, and one is tempted to demand that at k_0 the model displays an enstrophy flux equal to F_S^*. Then the right-hand side of Eq. (3.4) is always equal to F_S^*. If the model

is able to maintain the equilibrium spectrum, which is a k^{-3} energy and a k^{-1} spectrum for the enstrophy in the inertial range of two-dimensional turbulence (e.g., Kraichnan 1967), doubling the resolution allows for a reduction in dissipation with a factor between 8 and 16 according to Eq. (3.4).

So far the enstrophy flux has been considered. However, the existence of a viscous subrange necessitates an energy flux that decreases to zero in the viscous subrange to balance the energy dissipation. If ΔF_S remains constant, when enlarging the resolution, ΔF_E will become smaller and smaller. The equilibrium spectrum cannot fulfill this condition, and as a result an increased energy and enstrophy cascade to smaller scales arises to create a flatter spectrum at the short-wave end. As a matter of fact, Fox and Orszag (1973) demonstrated that without dissipation the truncated equations have a spurious equilibrium solution with a k^{+1} enstrophy and a k^{-1} energy spectrum. Bennet and Haidvogel (1983) showed that with too weak dissipation the turbulent system slowly spins down, but is never too far away from the spurious equilibrium.

An alternative would be to demand that ΔF_E is always constant. Assuming the equilibrium spectrum, this would result in a reduction of the dissipation with a factor between 2 and 4 when doubling the resolution. However, if the resolution is increased while ΔF_E remains constant, ΔF_S will become larger and larger. Again, this condition cannot be fulfilled by the equilibrium spectrum. The result is now a steeper spectrum within the viscous subrange. Whenever the viscous subrange is not too large (which would be the result of even stronger dissipation), this result is not too embarrasing. So a reduction factor that is as large as possible should be used to keep an inertial and a viscous subrange within the model solution. From the former arguments we anticipate that the reduction factor should be about 4.

Until now we only considered two-dimensional turbulence. According to Charney (1971), results from two-dimensional turbulence can be extended to three-dimensional quasigeostrophic flows, where the kinetic energy and enstrophy are replaced by the potential enstrophy and total energy. (As a matter of fact, one has to separate the energy into kinetic and potential energy and the enstrophy into relative and thermal enstrophy, and treat the friction and diffusion separately, but the reasoning remains the same.)

In three-dimensional flows quasigeostrophic scales are modified by ageostrophic effects. Most three-dimensional flows produce a spectrum with an inertial range somewhere between k^{-3} and k^{-4}. [See Rhines (1976) for a review of the subject.] Figure 1 shows the kinetic energy spectrum at day 30 for the standard experiment, confirming that it has an inertial range with broadly a k^{-3} spectrum and a steeper viscous subrange.

To test the arguments presented above, we have tuned the reduction factor while varying the resolution between 4 km $< dx <$ 28 km, demanding that ring formation should occur and resemble the standard experiment in Drijfhout (1990) as much as possible, and that the energy and enstrophy spectra should be altered as little as possible when changing the resolution and the dissipation parameters.

FIG. 1. Kinetic energy spectrum at day 30 in 10^{-3} m^3 s^{-2}.

We require that the dissipation should vary with resolution as $f(dx/10\text{ km})$. (The choice of 10 km as a scaling length is arbitrary, and results from the fact that the 10-km experiment was labeled as the standard experiment. The scaling length does not influence the functional dependency of the dissipation on the resolution.) The tuning process suggests the dissipation should vary with $(dx/10\text{ km})^{5/3}$. This means a factor 3.2 reduction with a doubled resolution. [Factors of about three were also used by Semtner and Mintz (1977), Cox (1985), and Böning (1989).] We have chosen to keep the ratio of the diffusion to the friction parameter constant to a value of 3, as usual in eddy-resolving experiments. To obtain the most consistent series with a dissipation varying as $(dx/10\text{ km})^{5/3}$, the dissipation has been slightly increased in the standard experiment compared to that of Drijfhout (1990) (two-layers, 10-km-horizontal resolution, biharmonic friction) with a factor of 1.2, giving $B_M = 1.2 \times 10^{10}$ m^4 s^{-1} and $B_T = 3.6 \times 10^{10}$ m^4 s^{-1}.

These changes have only a slight effect on the flow-field evolution and the higher-order statistics that are of interest. Therefore, the description of the physics controlling ring formation in the standard experiment in Drijfhout (1990) holds unchanged for the standard experiment here, and we shall use the former text as a reference.

b. *Horizontal resolution*

In Fig. 2, the sensitivity of the Cartesian primitive equation model to the resolution, as indicated by the basin-averaged heat transport and eddy kinetic energy level during ring genesis [averaged over the life cycle of the baroclinic disturbance, see Drijfhout (1990)], is displayed. A curve with a maximum at 10-km resolution is seen. This suggests that there are two competitive mechanisms working. The left wing of the curve, where the heat transport increases, is easily understandable. The model tries to simulate an energy conversion from the mean flow to ringlike structures on the scale of the internal Rossby radius (29.2 km). The success of this simulation depends on how well this scale is resolved. With a resolution much coarser than the Rossby radius, the model produces only a growing meander but no ring formation. With a resolution of 40 km > dx > 20 km the model simulates ring formation, but the rings are weak and they are quickly reabsorbed by the mean flow. Up to dx = 10 km both the reduction in explicit viscosity and the participation of smaller wavelengths contribute to enhance the growth of the most unstable wave with a 320-km wavelength.

The right wing of the curve of Fig. 2 is more puzzling at first sight. From 10 km to higher resolution the heat transport decreases: at 5-km resolution it is less than 50% of the heat transport at 10 km. When the flow evolution in these resolution experiments is carefully examined, we observe that the growth of the 320-km wave is monotonically enhanced when increasing the resolution (Fig. 3). The reduction of explicit dissipation contributes to this increase, while the additional short waves do not act to dissipate energy to the same extent. However, as shown in Fig. 3, the smaller wavelengths responsible for the process of backward breaking of the meander leading to the subsequent ring formation also display an enhanced growth. Moreover, they cause this "wavebreaking" to occur earlier, resulting in a weaker ring displaced closer to the mean jet. To understand this more completely we have to examine the process of "wavebreaking" in detail.

Robinson et al. (1988) and Drijfhout (1990) discussed the breaking process and ring formation in terms of a budget analysis of energy and vorticity. Pratt and Stern (1986) discussed this from a more theoretical point of view using contour dynamics.

The initial Rossby wave consists of a negative vorticity anomaly in the ridge of the wave and a positive vorticity anomaly in the trough. Due to the horizontally sheared flow in the jet, the top of the ridge (trough)

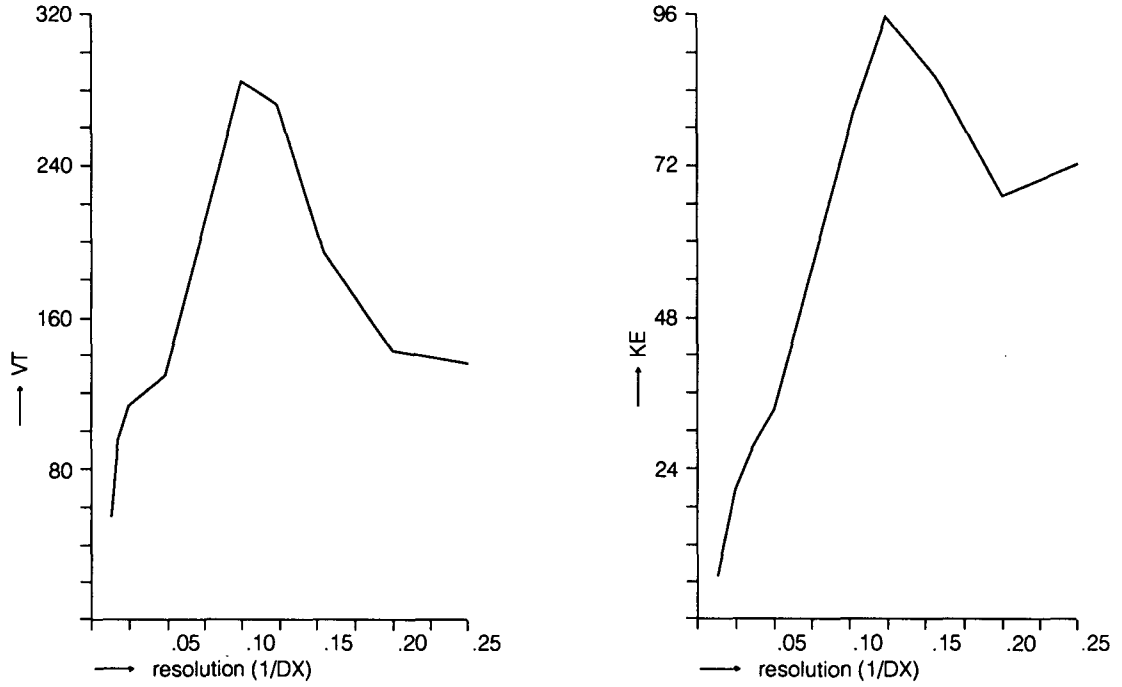

FIG. 2. Heat transport and eddy kinetic energy level as a function of resolution in 10^{-3} m^{-1}, KE is in 10^{-3} m^3 s^{-2}, VT in 10^{13} watt.

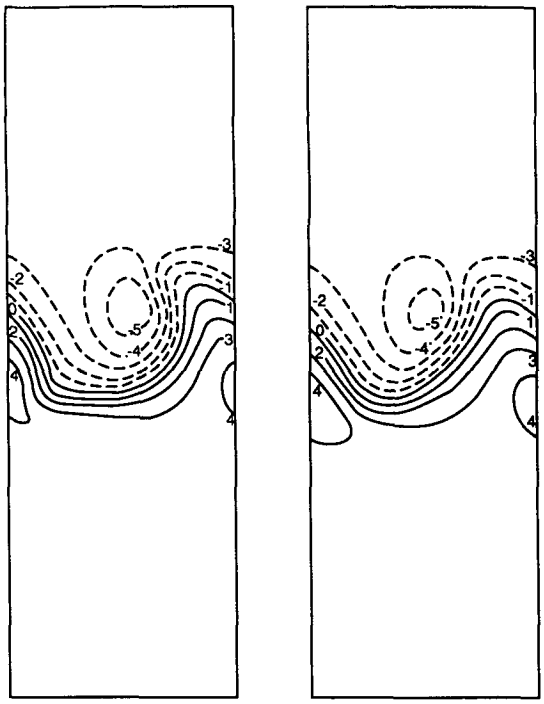

FIG. 3. The pressure field in the upper layer for the experiments with a horizontal resolution of 5 km (left) and 10 km (right). Contour differences are 0.667 $m^2 s^{-2}$.

will stay slightly behind (see Fig. 4). This induces at the upstream side of the ridge positive vorticity, which partly spills over the edge of the ridge and organizes itself into an opposite vortex in the wake of the ridge. (A similar story holds for the trough.) At the upstream side of the ridge (trough) the opposite vortices induce an extra upward (downward) motion, and the Rossby wave, or vorticity front, steepens at the upstream side. As this vortex-induced steepening primarily affects the vorticity front, streamlines show a less steeper wave than potential vorticity contours (compare Fig. 3 and Fig. 4). Thus, at the steeper upstream side, the vorticity front is crossed by velocity vectors. This causes the upstream side of the meanders to move faster downstream than the downstream sides. Consequently, the meander is narrowing and water within the meander flows back to the base. At the extremes, water is held back in the flow field of the opposite vortex and the opposite vortex "sucks" a blob of meander water through the thinning neck. This blob eventually becomes the pinched-off ring.

The question remains as to what accelerates this process or slows it down. As contour lines are packed more tightly where the front steepens, the potential vorticity gradient is locally enhanced (Fig. 4). Any form of diapycnal mixing of potential vorticity will reduce this gradient and, consequently, the steepening of the front. So the diapycnal mixing counteracts the process of Rossby wave steepening and causes the meander to reach larger amplitudes before ring formation occurs. We hypothesize that the larger diapycnal mixing at 10-km resolution compared to 5 km is to first order responsible for the heat transport difference. In the following experiments this hypothesis is tested further.

c. *Vertical resolution*

The effect of including higher-order vertical modes is unknown beforehand; it could work either way. On one hand, the better resolved jet profile could increase the instability of the flow. On the other hand, if the vertical resolution is increased, the diapycnal mixing decreases. In that case, our hypothesis predicts that in a four-level model wave breaking will occur at an earlier stage. Consequently, the heat transport should be less than in a two-level model.

To test this hypothesis, we have extended the standard model, with 10-km resolution in the horizontal, to a four-level model. However, keeping the first internal Rossby radius constant, we have many degrees of freedom to choose the vertical structure of a four-level model. We experimented with a series of different profiles. In all experiments, the ultimate meander amplitudes and heat transport are less than in the two-level model. The four-level run that yields the largest eddy kinetic energies and heat transport will be described; i.e., where the influence of the higher-order vertical modes is minimal. The parameters for this experiment are

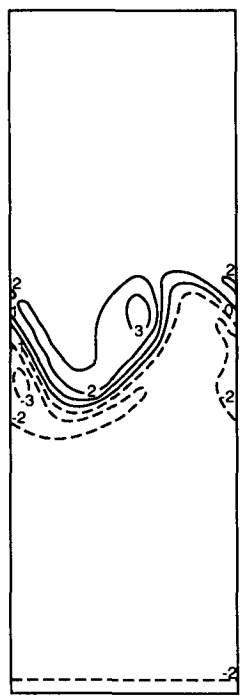

FIG. 4. The potential vorticity field at day 20 for the standard experiment. Contour differences are 1.5×10^{-5} s^{-1}.

$H_1 = 200$ m, $H_2 = 400$ m,

$H_3 = 800$ m, $H_4 = 2800$ m,

$U_1 = 120$ cm s^{-1}, $U_2 = 80$ cm s^{-1},

$U_3 = 50$ cm s^{-1}, $U_4 = 12$ cm s^{-1},

$g'_1 = g'_2 = g'_3 = 0.51$ cm s^{-1}.

In Fig. 5 the meander growth for the two-level and four-level model are compared. We see that wave growth is slightly enhanced in the four-level run. The dominating effect, however, is the earlier breaking of the ridge into a warm-core ring, smaller than the warm-core ring, that in a later stage will be pinched off in the two-level model. A comparison of the heat transport in both models confirms this picture. In the beginning the heat transport in the four-level model increases faster, but this is offset by a quick reduction after it has reached its maximum at day 25. The overall heat transport is 80% of the heat transport in the two-level model, although the flow is more unstable. This result is in agreement with the hypothesis that the spurious diapycnal mixing retards the processes of Rossby wave breaking, which causes ring formation to occur at larger meander amplitudes, resulting in a spuriously enhanced heat transport.

If we increase the vertical resolution further the spurious diapycnal mixing in the Cartesian model will decrease. However, it cannot be solved, as the mixing still occurs within horizontal surfaces. Also the effect of the increase of the vertical resolution will depend on the horizontal resolution, the basic state, and the nonlinearity of the processes with which the spurious diapycnal mixing interferes. For the standard model with 10-km resolution, increasing the vertical resolution to more than four levels does not change the effect of the spurious diapycnal mixing significantly.

4. The closure formulation

a. Biharmonic friction

In this section the sensitivity of the Cartesian model to variations in the friction and diffusion parameters is explored. In one set of experiments we keep the ratio of the diffusion to the friction parameter constant at a value of 3. This value is commonly used in eddy-resolving primitive equation models (e.g., Semtner and Mintz 1977; Cox 1985; Böning 1989). The diffusion and friction parameters have been varied separately. Other parameters are equal to the standard experiment.

Offhand, we expect that increasing these parameters results in a damping of the growth of the 320-km wave, ultimately leading to saturation before ring formation occurs. From a certain point onward, the heat transport will decrease with increasing damping. On the basis of the hypothesis formulated earlier, however, it is expected that the reduction in diapycnal mixing, when

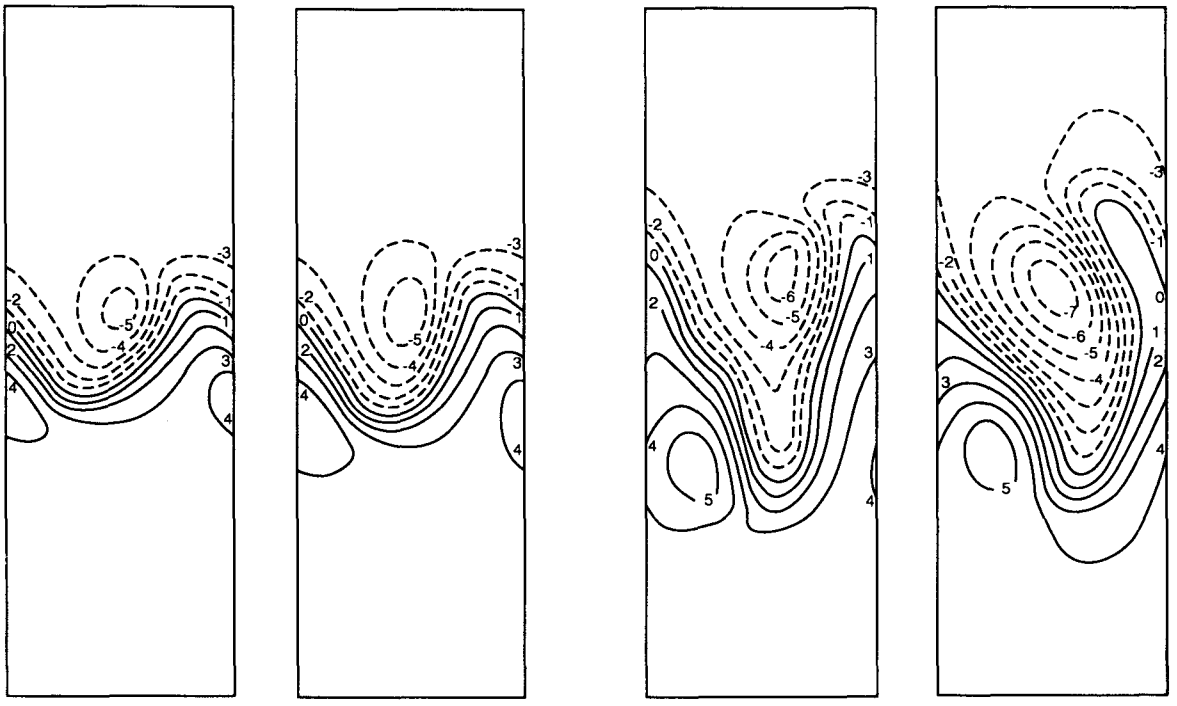

FIG. 5. Pressure fields at day 20 (extreme left) and day 30 (extreme right) for the two-level (left) and four-level (right) experiment.

decreasing the dissipation parameters, will result in earlier wave breaking and also in a reduced heat transport. From these arguments the heat transport, as function of the dissipation parameters, is expected to display a distinct maximum. However, the reduction of dissipation also causes the smallest scales to attain more enstrophy and to a lesser extent more energy. These smaller wavelengths could alter the process of ring genesis, though it seems improbable that they will prolong the phase of meander growth and enhance the heat transport to such a degree that the expected maximum disappears.

Figure 6 shows a distinct maximum in heat transport when varying the dissipation. In Fig. 7, the potential vorticity field at day 20 is seen for the standard experiment and for the experiment with dissipation reduced by a factor of 3.2. We observe that at roughly the same wave amplitude, the degree of wave steepening is enhanced. At day 30 it is observed that ring formation is taking place in the lower dissipation case, at a time when the standard experiment still shows a growing meander. This meander has reached considerably larger amplitude, although the initial wave growth in the standard experiment was smaller. Therefore, these experiments confirm that the spurious mixing of potential vorticity retards wave breaking and consequently enhances the heat transport.

In all experiments leading to Fig. 6, rings were formed. Figure 8 displays this process for the experiment with the highest dissipation (enhanced by a factor 10). The maximum amplitude, reached at day 40, is considerably smaller than in the standard experiment. At day 50 we observe an immensely tilted meander neck indicating that the time needed for the cutoff process is prolonged dramatically. Although the dissipation parameters are enhanced by a factor of 10, locally in the neck the amount of vorticity dissipation during the ring cutoff is reduced almost by a factor of 10 due to the weakened vorticity gradients. The enstrophy cascade, which is important for closing the potential vorticity contours in the neck region, is consequently slowed down.

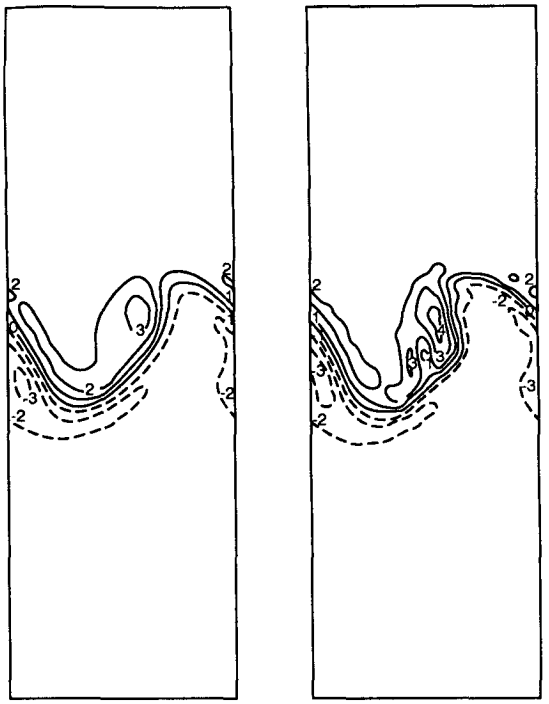

FIG. 7. The potential vorticity field at day 20 for the standard experiment (left) and the low-dissipation experiment (right).

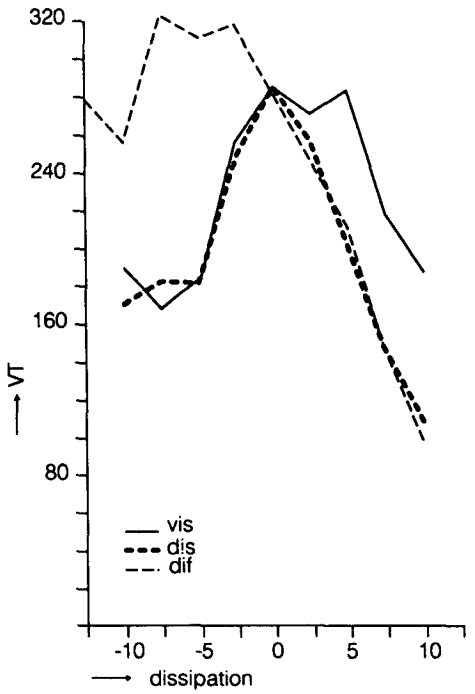

FIG. 6. The heat transport as a function of the dissipation parameters. The logarithmic scale ranges from 10^{-1} to 10^{1} times the standard value. DIS denotes both viscosity and diffusivity parameters are changed.

From Fig. 6 it can also be concluded that both diapycnal mixing of momentum and that of density are important in increasing the heat transport. This can be understood since both the mixing of momentum and of density results in mixing of potential vorticity, which retards the process of ring formation, resulting in larger rings. We see that with larger dissipation damping through diffusion is stronger; a strong diffusion decreases the available potential energy by leveling off temperature gradients. The experiments show further that for small values of dissipation, the model is more sensitive to the viscosity parameter. The ratio of relative to thermal vorticity increases with wavenumber, similar to the ratio kinetic to potential energy, which display a k^{-3} respectively a k^{-5} spectrum for large wavenumbers (see Rhines 1976). Therefore, the small-scale enstrophy is dominated by the relative vor-

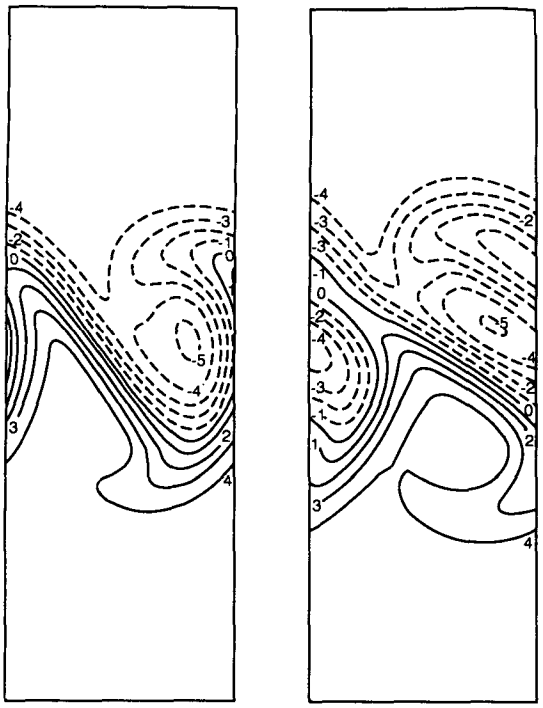

FIG. 8. The temperature field at day 40 and day 50 for the high-dissipation experiment. Contour differences are 0.4 K.

ticity field, which is controlled by the viscosity parameter.

The strong sensitivity of the Cartesian primitive equation model to the dissipation parameters is in agreement with the results of Holland and Batteen (1986), who also found that quite small changes in the horizontal diffusivity substantially modified the baroclinic flow field in an eddy-resolving quasigeostrophic model.

b. *Laplacian friction*

Holland (1978) introduced the biharmonic friction parameterization because it operates far more scale selective than the Laplacian friction used so far in ocean models. In this section, we compare the simulations that use biharmonic friction to simulations with Laplacian friction. The results will also be used as a reference for the next section, where the effect of rotation of the dissipation tensors in a Cartesian model to isopycnal coordinates is explored.

Two experiments will be discussed. The first is a run with a friction parameter A_M of 1.2 10^2 m^2 s^{-1}, a diffusion parameter A_T of 3.6 10^2 m^2 s^{-1}, and other parameters equal to the standard experiment. The second experiment uses a two times weaker dissipation. Both experiments yield less energy conversion than the biharmonic friction experiment, although the low Laplacian friction run was selected as the experiment that yields the largest eddy energy and heat transport for all values of this type of parameterization. In the experiment with doubled dissipation, the energy conversions and heat transport fall a factor of 2 below the standard experiment: the dissipation of mean available potential energy is considerable.

In Fig. 9 (displaying the potential vorticity fields just before ring cutoff) we see that the low dissipation case produces much more small-scale enstrophy than the biharmonic experiment. These experiments demonstrate the lesser scale selectivity of Laplacian friction; reducing the small-scale enstrophy cannot be done without seriously affecting the mean available potential energy.

Noisy as it is, the experiment with weak dissipation will be used as a reference for the next section, in which the dissipation tensors to isopycnic coordinates are rotated. The rotation is only numerically tractable for Laplacian friction. We demonstrate the effect of reducing the diapycnal mixing for the experiment with maximum heat transport, as this experiment most closely resembles the standard experiment with biharmonic friction. Moreover, the effect of the spurious diapycnal mixing will be largest in the experiment with maximum heat transport.

c. *Mixing tensors in isopycnal coordinates*

The type of closure formulation used has the effect of fluxing density and momentum across isopycnals.

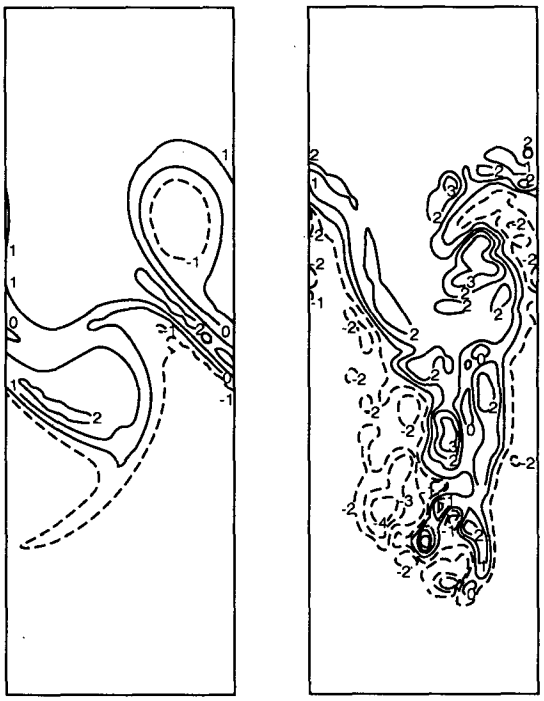

FIG. 9. The potential vorticity field for the Laplacian friction experiments just before ring cutoff. Left shows the high-dissipation experiment, right the low-dissipation run.

In the Cartesian reference frame, mixing of density and momentum occurs strictly along horizontal and vertical coordinates, while isopycnals are inclined. Since most of the lateral mixing occurs along isopycnals, rather than in horizontal surfaces (McDougall and Church 1986), it would be desirable to parameterize the lateral mixing to be effective along isopycnals. Since the introduction by Redi (1982) many have applied this type of mixing, some have developed even more refined parameterizations (e.g., McDougall 1987; Gent and McWilliams 1990). In this section we follow the principles outlined by Redi (1982), which were further developed to be incorporated in numerical models by Cox (1987).

First, the results when only the diffusivity tensor is rotated are discussed. Figure 10 displays the potential vorticity fields at day 20 with horizontal and isopycnal diffusion. In the latter case we see that the Rossby wave is steeper at roughly the same amplitude. This is in agreement with our hypothesis about the effect of diapycnal mixing on wave breaking. Consequently, the heat transport is reduced (75% compared to horizontal mixing) as eddy cutoff occurs at an earlier stage of wave growth.

When both the diffusivity and viscosity tensor are rotated, the initial flow development is similar to the case with rotating the diffusivity tensor alone; apparently the reduction in wave steepening mainly occurs through the diapycnal mixing of density. However, between day 30 and day 40 the flow evolution in the two experiments starts to diverge (Fig. 11). Rotation of the viscosity tensor now substantially shortens the eddy cutoff process and the period of large energy conversions and heat transport. Figure 11 already shows that the ring in the experiment with horizontal viscosity will be larger and displaced further southward than the ring in the experiment with both diffusivity and viscosity operating along isopycnals.

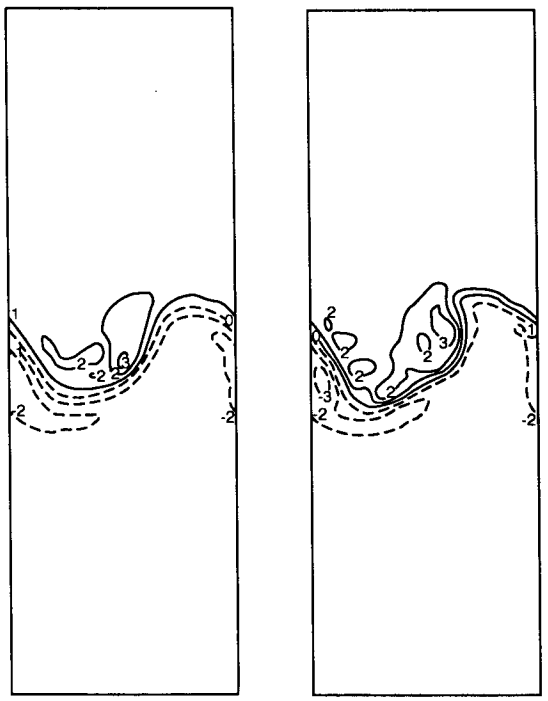

FIG. 10. Potential vorticity field at day 20 for the experiment with horizontal diffusion (left) and isopycnal diffusion (right).

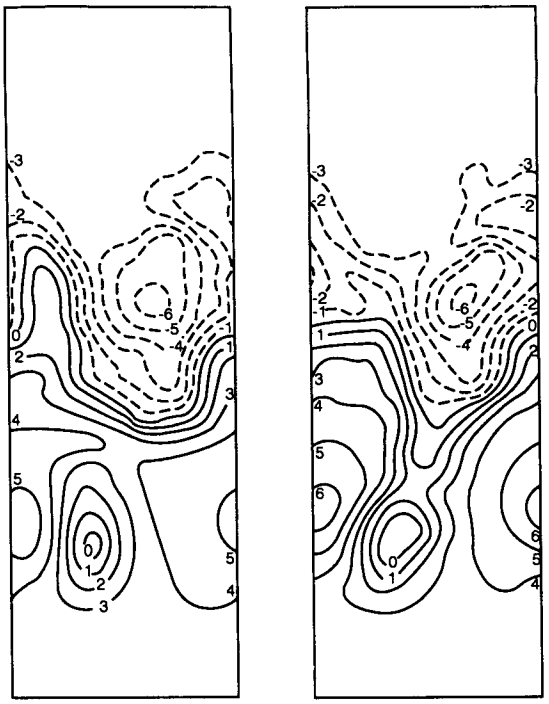

FIG. 11. The pressure field at day 40 for the experiment with isopycnal diffusion only (left) and the experiment with both isopycnal diffusion and viscosity (right).

Whereas the effect of the diapycnal mixing of density was seen to retard the wave breaking, the effect of the diapycnal mixing of momentum appears to retard the enstrophy cascade in the neck of the meander by weakening the vorticity gradients. This results in a prolonged phase of the cutoff process; the opposite vortex is able to "suck" more fluid through the neck, and the ring that is ultimately formed will be larger.

The experiment with both the viscosity and diffusivity tensors rotated yields a heat transport that is 60% of the experiment with horizontal mixing, compared to 75% when only the diffusivity tensor is rotated. When rotating the viscosity tensor alone, the heat transport is slightly enhanced, compared to horizontal mixing. This behavior stresses the nonlinear character of the process, where small effects can give large and unpredictable results.

We conclude that the effect of rotating the lateral mixing to take place along isopycnals enhances wave breaking and reduces the heat transport, in agreement

with the hypothesis formulated in section 3. As both diapycnal fluxes of density and momentum affect the potential vorticity of the flow, it is necessary to rotate both the diffusivity and viscosity tensors to get a reduction in heat transport comparable with the observed overshoot in the nonrotated case at 10-km resolution (Fig. 2).

5. A model comparison

a. Isopycnal versus Cartesian coordinates

To eliminate diapycnal fluxes of density and momentum due to subgrid-scale horizontal mixing, two approaches are possible. The first, rotating the diffusion and viscosity tensors, reduces this error significantly, but at the cost of a lot of extra computer time. This procedure becomes numerically intractable when biharmonic friction is used; as shown above, in eddy-resolving models where a more scale-selective dissipation is needed, the spurious diapycnal mixing still can have serious effects on the flow evolution. Truncation errors in the advection scheme also cause diapycnal fluxes, which cannot be eliminated from a Cartesian coordinate model. The alternative is to use a layered model where the isopycnals themselves are coordinate surfaces. Although these models have some problems with simulating the large-scale thermohaline circulation, namely, deep convection and water-mass formation, for many modeling purposes the layered model has a clear advantage (e.g., Bleck and Boudra 1986; Huang and Bryan 1987).

One of these advantages is demonstrated in Fig. 12, which shows the heat transport as a function of resolution for both the isopycnic and the Cartesian primitive equation model. The heat transport is now equated to the transport of a normalized pressure difference between the first and second layer:

$$T^* = (p_1 - p_2)/(ag\Delta z).$$

It is seen that the asymptotic value of the heat transport is already reached at $(dx)^{-1} = 0.05$, compared to 0.20 for the Cartesian model. The overshoot due to diapycnal mixing and the subsequent retarded wave breaking is absent in this model. There still is a small overshoot effect due to the fact that increasing the horizontal resolution increases the ability of the nonlinear flow field to create sharper gradients. The enhanced vorticity gradient augments the steepening of the Rossby wave and speeds up the wave-breaking process.

Within the Cartesian model two processes can be identified that are responsible for retarding wave breaking and the subsequent overshoot in heat transport at 10-km resolution: the spurious diapycnal mixing and an incomplete resolution of the vorticity gradient at the Rossby wave front. The latter effect is also present in the isopycnic model. In both models the overshoot in heat transport caused by an incomplete resolution of the vorticity front will be of the same order of magnitude. Comparing the heat transport difference be-

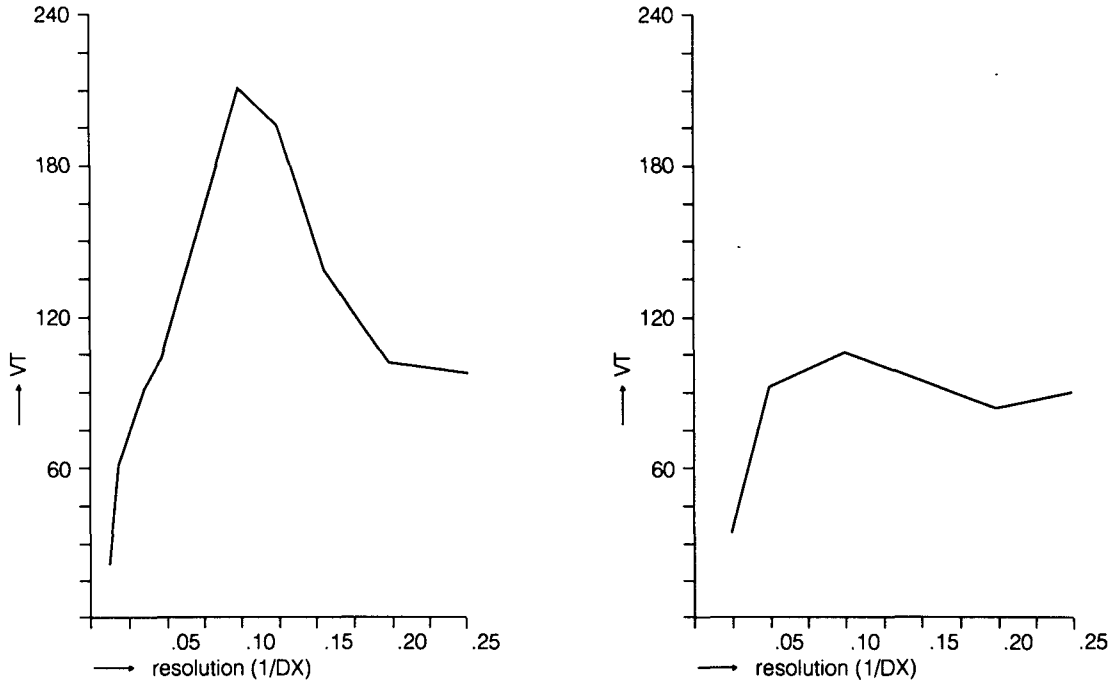

FIG. 12. Heat transport as a function of resolution for the Cartesian (left) and isopycnal (right) primitive equation model.

tween 10-km and 5-km runs in the Cartesian and isopycnic model, we can conclude from Fig. 12 that in the Cartesian model the overshoot mainly comes from the spurious mixing and that the retarding of wave breaking due to the absence of smaller scales is a lesser effect.

If ring genesis as simulated by the isopycnic model is compared with the standard experiment of the

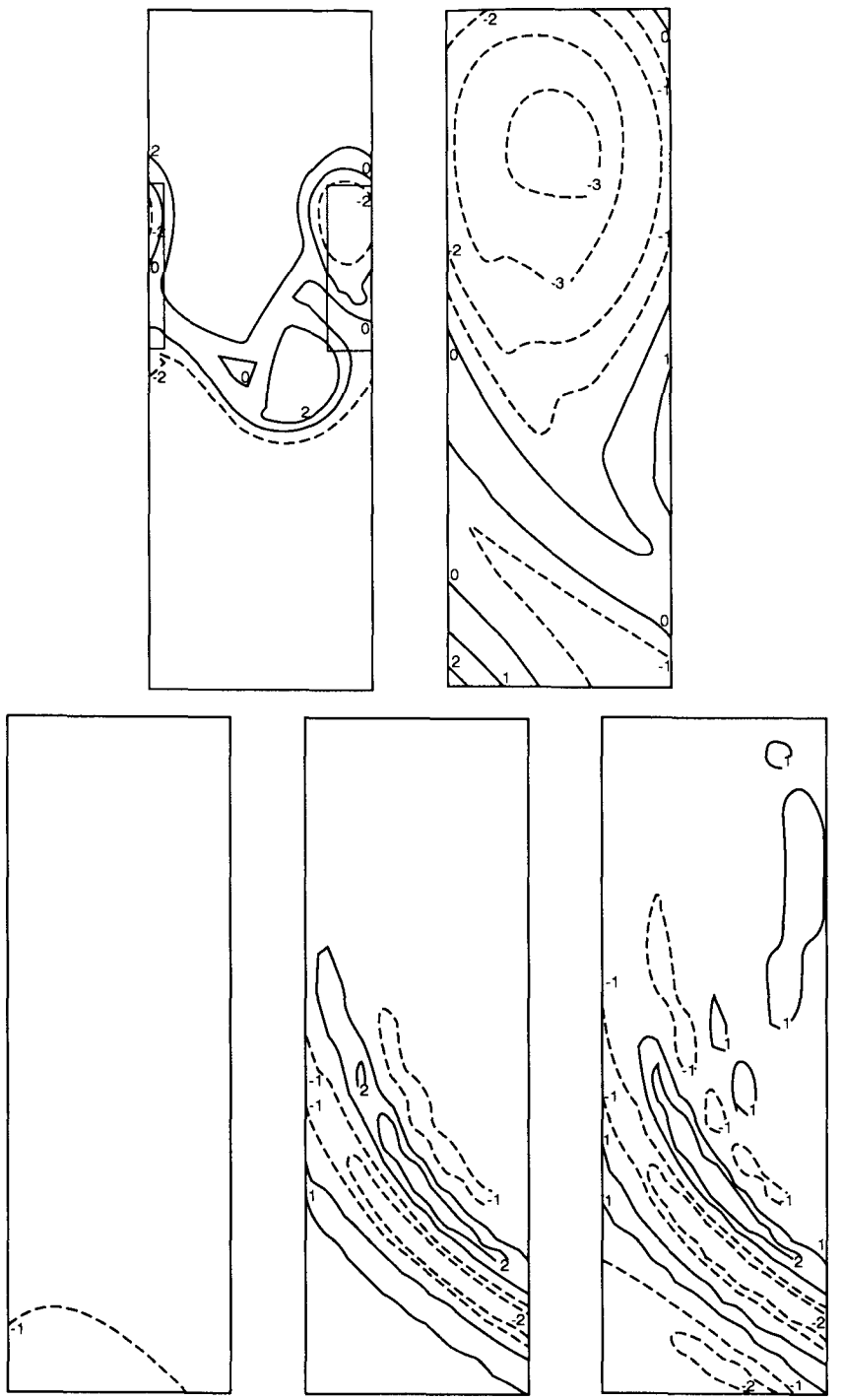

FIG. 13. The potential vorticity field at day 59 for the model domain and the subdomain indicated (above), showing the standard run with the isopycnal model. Below, the Lagrangian vorticity budget at day 59 for the subdomain. From the left to the right: fw_z, $B_M\nabla^4\xi$, and $d\xi/dt$. Contour differences are 10^{-12} s^{-2}.

Cartesian model, we find that in general the physics of ring genesis, studied by Drijfhout (1990), with an energy and vorticity analysis and the process of wave breaking described in Section 3 are qualitatively the same for the two models studied. Figure 13 shows the Lagrangian vorticity balance just before the warm ring cutoff for the isopycnic model at 10-km resolution. Within the Cartesian model vortex stretching due to the differential advection of a smaller wave dominates the Lagrangian vorticity budget, while in the isopycnic model the vorticity dissipation is dominant. This is due to the fact that in the isopycnic model no cold-core ring is formed—the process that induced the smaller wave in the Cartesian model (see Drijfhout 1990). But from all experiments done with the Cartesian model, varying closure parameterization and resolution, we conclude that ring cutoff due to vorticity dissipation is far more general than a cutoff caused by the differential advection of a smaller wave.

It is concluded from these experiments that the sensitivity to resolution of the Cartesian model is much larger than for the isopycnic model. The hypothesis on the effect of the spurious diapycnal mixing on the simulation of ring genesis is in agreement with results from the isopycnic model.

b. The nonpotential vorticity-conserving advection scheme

As mentioned in the Introduction, two spurious processes are present in the Cartesian model; diapycnal mixing and a non–potential-vorticity–conserving advection scheme. The latter effect is responsible for an enhancement of the extreme values in the potential vorticity field. During ring genesis, the initial difference in potential vorticity across the Rossby wave front increases with time and is ultimately doubled in the standard experiment. This enhancement of potential vorticity extremes is caused by the increase of vorticity anomalies both in the ridge and through of the wave and in the opposite vortices. This results in enhanced wave growth.

Figure 14 compares the potential vorticity fields for the isopycnic and Cartesian primitive equation model. This figure illustrates the enhanced wave growth in the Cartesian model. However, the heat transport is not increased by this process. The non–potential-vorticity–conserving advection scheme causes the ring genesis to proceed faster but without altering the relative duration of the different phases. With a resolution of 5 km, ring formation occurs at the same meander amplitude for the isopycnic and Cartesian model. Although ring genesis proceeds about twice as fast in the Cartesian model, the heat transport is the same for both models; see Fig. 12.

As the enhancement of potential vorticity extremes becomes more prominent in the Cartesian model when resolution is increased, it is questionable whether the two models will converge to the same solution at very high resolution. Spuriously generated potential vorticity extremes at the small scales could, at still higher res-

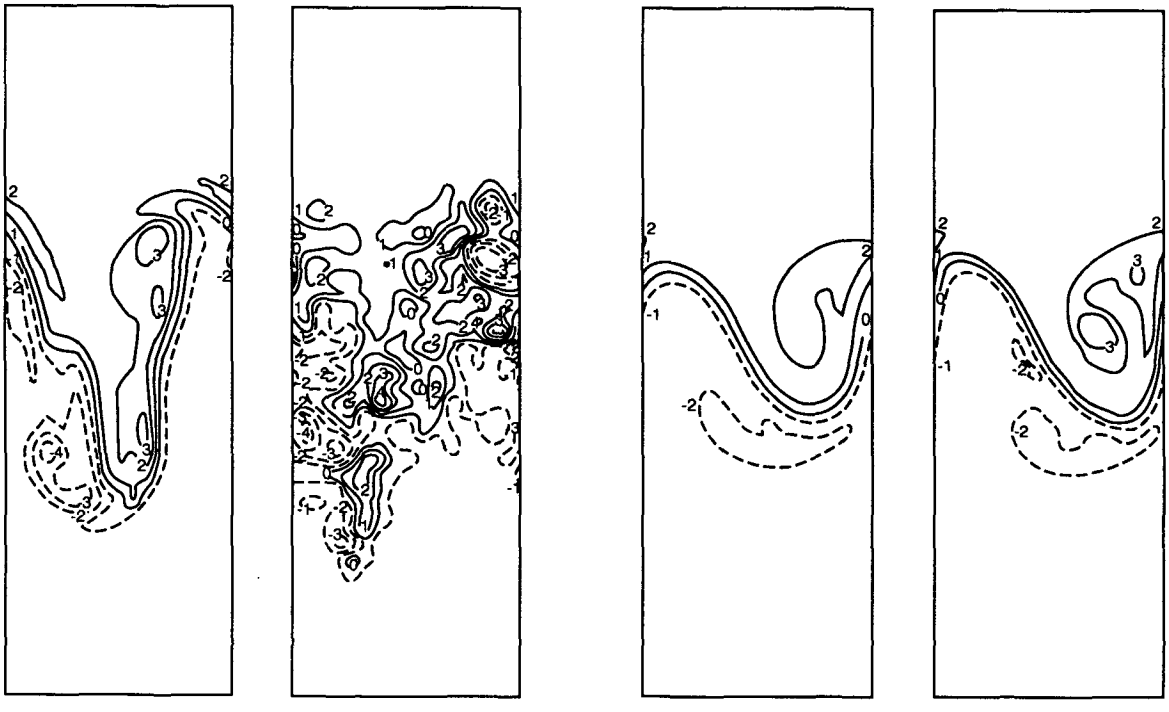

FIG. 14. The potential vorticity field at day 30 for a standard (left) and low (right) dissipation run with, respectively, the Cartesian (extreme left) and isopycnic (extreme right) primitive equation models.

olution, even come to dominate the process of ring genesis.

Moreover, as a result the Cartesian model becomes increasingly sensitive to changes in the dissipation parameters, while this is not the case for the isopycnic model. Figure 14 illustrates this by comparing flow fields of both models with standard values for diffusivity and viscosity and with these parameters reduced by a factor of 10. The Cartesian model becomes overwhelmed with small-scale vorticity structures, while this is not the case in the isopycnic model. This is the result of the potential vorticity–conserving advection schemes.

The use of higher-order formulations could possibly reduce errors due to the non–potential-vorticity–conserving advection scheme. Furthermore, not only the closure parameterization but also the advection scheme causes spurious diapycnal fluxes as a result of truncation errors and consequent phase errors in the various wave components. Therefore, we performed an experiment with fourth-order advection schemes in the momentum and density equations to test whether the use of higher-order schemes can reduce the errors within the Cartesian model. The higher-order formulations were only applied for the horizontal advection terms; they do not affect the energy-conserving properties of the model. The formulation follows the treatment of the advection in the density equation by Bleck and Boudra (1986).

Results show little effect compared to the standard experiment; the reduction in heat transport is less than 5%. The flow evolution in this experiment is in agreement with the earlier observation that the non–potential-vorticity–conserving advection schemes enhance wave growth, while they do not contribute to processes responsible for a heat transport overshoot. The increase of potential vorticity extremes is somewhat reduced, and the whole process of ring genesis develops slower, but meanders reach the same amplitude before breaking and ring formation occurs.

In conclusion, the use of higher-order advection schemes cannot eliminate the errors due to a non–potential-vorticity–conserving advection scheme. Furthermore, the diapycnal mixing of potential vorticity due to truncation errors in the advection schemes is negligible compared to the diapycnal mixing due to a horizontal closure formulation.

c. Quasigeostrophic versus primitive equation

As quasigeostrophic models are much less time consuming than primitive equation models and, moreover, the quasigeostrophic equations often produce realistic results far beyond the range of their formal validity, a comparison between quasigeostrophic and primitive equation simulations of various processes in fluid dynamics has been a subject of research for a long time (e.g., Semtner and Holland 1978; Spall and Robinson 1990). The latter authors even report, although the quasigeostrophic model had incomplete physics, a better SST hindcast with the quasigeostrophic model.

Figure 15 shows the heat transport for the quasigeostrophic model as a function of resolution. This can be compared with Fig. 12. It is seen that the overshoot effect due to a spurious diapycnal mixing is considerably less than in the case of the Cartesian primitive equation model. The process of Rossby wave steepening is a nonlinear process at such small scales so that ageostrophic effects are important. Quasigeostrophic physics do not describe these effects correctly, and consequently the spurious diapycnal mixing affects the process of wave steepening and wave breaking in a quasigeostrophic model much less. Compared to the Cartesian primitive equation model, the quasigeostrophic model gives better results regarding the heat transport, but for the wrong reason.

Since within the Cartesian primitive equation model wave growth is enhanced by spurious potential vorticity creation, we compare the wave growth with the isopycnic model. Wave growth proceeds faster in the quasigeostrophic model; apparently the ageostrophic modes slow the growth of the meander. This feature was also found by Spall and Robinson (1990). However, it is also clear that wave steepening and wave breaking proceeds much slower in the quasigeostrophic model; at the same meander amplitude the absence of smaller-scale processes in the quasigeostrophic model is striking.

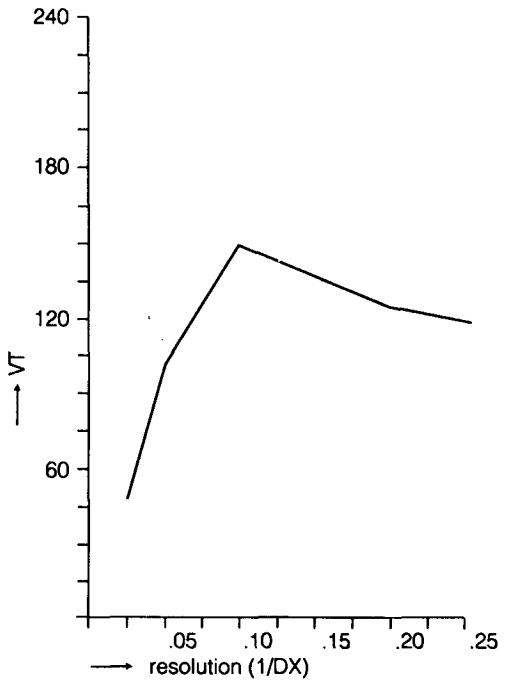

FIG. 15. The heat transport as a function of resolution for the quasigeostrophic model.

As increased resolution hardly enhances wavebreaking in the quasigeostrophic model, this model yields at 5-km resolution, larger heat transports than the two primitive equation models described. We conclude from the experiments with the quasigeostrophic model that it suffers from inadequate physics with respect to small-scale (ageostrophic) processes such as Rossby wave steepening, wave breaking, and ring cutoff. As a matter of fact, ring cutoff in this model simulation did not occur at all (see Fig. 16), although with a more unstable jet profile this process can be simulated by a quasigeostrophic model (e.g., Ikeda 1981; Robinson et al. 1988).

An advantage over Cartesian primitive equation models is the potential vorticity–conserving character of the model and the resulting lack of sensitivity to the dissipation parameters, if not chosen too large. Small-scale enstrophy in a quasigeostrophic model is less than within a primitive equation model, as primitive equation physics contain more instability mechanisms and admit higher Rossby number flow (e.g., Spall and Robinson 1990). As a result, a reduction by a factor 10 of the dissipation parameters proved to have hardly any effect in the quasigeostrophic model, higher-order statistics being changed by less than 5%.

6. Discussion and conclusions

The purpose of this study has been to evaluate the role of resolution, closure formulation, and model formulation in simulating ring genesis, particularly with respect to the transport of heat. The role of spurious diapycnal mixing of heat and momentum and of the non–potential-vorticity–conserving character of the advection schemes has been demonstrated in Cartesian primitive equation models. The extent to which quasigeostrophic dynamics are capable of describing the process of ring genesis was also tested.

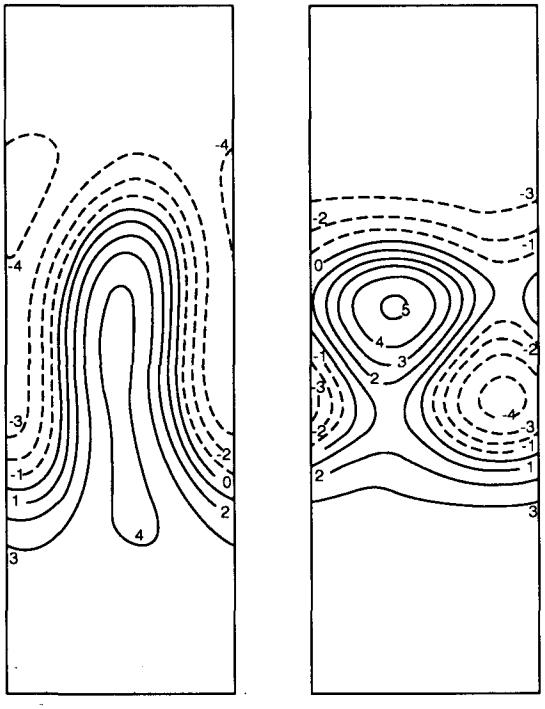

FIG. 16. The pressure field for the quasigeostrophic model at days 80 and 100.

Varying the horizontal resolution, it was found that Cartesian primitive equation models display a distinct maximum in heat transport. At 10-km resolution, it is two times as large as at 5-km resolution. We hypothesized that this overshoot effect can be explained as a result of the spurious diapycnal mixing of heat and momentum, acting to reduce the potential vorticity gradient at the Rossby wave front. This results in retarding the processes of wave steepening and wave breaking and in a prolonged growth of the meander.

In general, such a hypothesis cannot be verified, but a series of experiments was performed that could falsify the hypothesis if untrue. However, all experiments showed results in agreement with the prediction from this hypothesis. It has been made likely that Cartesian model results can seriously be affected by spurious diapycnal mixing. In particular, this has been demonstrated for the simulation of ring genesis and the subsequent heat transport in eddy-resolving models.

When varying the strength of the dissipation parameters (diffusivity and viscosity), a maximum in heat transport was found. Again the decrease in heat transport can be explained by the reduced spurious diapycnal mixing. Decreasing the dissipation parameters acts to speed up the process of wave breaking.

Using Laplacian instead of biharmonic friction, we were not able to reduce the amount of small-scale enstrophy to a level comparable to the standard experiment with biharmonic friction without seriously affecting the mean available potential energy. The experiment with Laplacian friction that yielded the largest heat transport was used as a reference to compare the effect of rotating the diffusion and friction tensors to isopycnic coordinates.

It turned out to be necessary to rotate both the diffusion and friction tensors to isopycnic coordinates. The reduction in heat transport when rotating the diffusion tensor only is 25%, while after rotating both the diffusion and friction tensors this reduction becomes 40%. As the diapycnal flux of both density and momentum contribute to a diapycnal potential vorticity flux, they both change the dynamics of ring genesis. The diapycnal flux of density appears to be most important in reducing wave steepening and retarding wave breaking, while the diapycnal flux of momentum modifies the cutoff process at a later stage.

The overshoot effect in heat transport found in the Cartesian primitive equation model is an order of magnitude smaller in the isopycnic and quasigeostrophic model. This feature is in agreement with the

hypothesis that, to first order, the overshoot is caused by spurious diapycnal mixing in Cartesian models. Since the quasigeostrophic dynamics are not able to simulate the process of wave steepening and wave breaking adequately, spurious diapycnal mixing has little effect in retarding the wave-breaking process in this case.

The non–potential-vorticity–conserving advection schemes were found to enlarge vorticity anomalies both in the ridge and trough of the Rossby wave and in the opposite vortices, resulting in enhanced wave growth. The heat transport in both the isopycnic and Cartesian model seems to converge from a resolution of 5 km down; however, due to the non–potential-vorticity–conserving character of the Cartesian model, the flow evolution remains quite different.

In general, we can conclude that the Cartesian primitive equation model is far more sensitive to resolution and closure formulation than both the isopycnic and quasigeostrophic models. We have demonstrated that Cartesian models suffer from inadequate physics due to the diapycnal fluxes of density and momentum. The quasigeostrophic model was not able to simulate the wave-breaking process correctly. The Cartesian primitive equation model is subject to additional spurious physics, resulting from the non–potential-vorticity–conserving advection schemes. Spurious contributions to the vorticity balance were found to increase with increasing resolution. This also causes the model to become increasingly sensitive to the strength of the dissipation parameters and to the closure formulation itself.

Although most of these experiments have been run with a two-level model in which the effect of the inadequate physics is stronger than in Cartesian models with a higher vertical resolution, the spurious diapycnal fluxes of density, momentum, and subsequently potential vorticity will not disappear when the resolution is increased. Moreover, the diapycnal flux of potential vorticity due to the non–potential-vorticity–conserving advection schemes increases with increasing horizontal resolution. Furthermore, when modeling the general ocean circulation, these spurious physics will interact with nonlinear processes, such as baroclinic and barotropic instability, which can result in large unpredictable effects.

To which extent the effects highlighted in this study will affect the simulated flow fields in ocean general circulation models is yet unclear. However, from this study it seems probable that in Cartesian models processes regarding eddy heat transport suffer from inadequate physics. Whether or not changes in the spurious diapycnal flux of density play a role in the heat budget in the eddy-resolving ocean models of Semtner and Mintz (1977) and Cox (1985), (partly) explaining the effect that the eddy heat transport is compensated by the heat transport difference of the changed mean flow, is yet unclear. A detailed comparison between an isopycnal and a Cartesian primitive equation closed basin model is needed to answer this question. This will be subject of the next study.

Acknowledgments. This research was supported by the European Economical Community (EEC) and the Netherlands Foundation for Pure Research (NWO). We acknowledge gratefully Arie Kattenberg, Theo Opsteegh, Gé Prangsma, and Will de Ruyter for comments on an earlier version of this manuscript and discussion from which this study benefited. Special thanks go to Rainer Bleck and Motoyoshi Ikeda for making their computer models available and explaining the source code in detail when necessary.

APPENDIX

Energy Budgets

We define $\Phi = \bar{\Phi} + \Phi'$, where $\bar{\Phi} = 1/D \int_0^D \Phi dx$, the zonally averaged value of any quantity Φ. This allows us to distinguish among K_m, K_e, P_m, and P_e; respectively, the mean kinetic energy, eddy kinetic energy, mean available potential energy, and eddy available potential energy. Labeling the equations, those with a subscript a refer to the primitive equations model, those with b to the isopycnic model, those with c to the quasigeostrophic model; h denotes the layer depth.

$$K_{m_a} = (\overline{u^2}/2 + \overline{v^2}/2)h \tag{A.1a}$$

$$K_{m_b} = (\overline{u^2}/2 + \overline{v^2}/2)h \tag{A.1b}$$

$$K_{m_c} = (\overline{u^2}/2 + \overline{v^2}/2)\partial\bar{p}/\partial s/g \tag{A.1c}$$

$$K_{e_a} = (\overline{u'^2}/2 + \overline{v'^2}/2)h \tag{A.2a}$$

$$K_{e_b} = (\overline{u'^2}/2 + \overline{v'^2}/2)h \tag{A.2b}$$

$$K_{e_c} = (\overline{\partial p/\partial s\, u'^2}/2 + \overline{\partial p/\partial s\, v'^2}/2)/g \tag{A.2c}$$

$$P_{m_a} = agh(\overline{T^2}/\bar{T}_z)/2 \tag{A.3a}$$

$$P_{m_b} = 1/g\partial\overline{p^2}/\partial s/2 \tag{A.3b}$$

$$P_{m_c} = h\overline{(\psi_2 - \psi_1)^2}F_1/2 \tag{A.3c}$$

$$P_{e_a} = ahg(\overline{T'^2}/\bar{T}_z)/2 \tag{A.4a}$$

$$P_{e_b} = 1/g\partial\overline{p'^2}/\partial s/2 \tag{A.4b}$$

$$P_{e_c} = h\overline{(\psi_2 - \psi_1)'^2}F_1/2. \tag{A.4c}$$

Lorenz (1955) derived equations for the various components of the energy budget of a geophysical fluid. In these equations the following terms can be distinguished (where $\{K_m, K_e\}$ denotes a conversion from K_m to K_e, etc.):

$$dK_m/dt = \{K_e, K_m\} - \{K_m, P_m\} - K_{m_{\text{dis}}} \tag{A.5}$$

$$dK_e/dt = \{P_e, K_e\} - \{K_e, K_m\} - K_{e_{dis}} \quad (A.6)$$

$$dP_m/dt = \{K_m, P_m\} - \{P_m, P_e\} - P_{m_{dis}} \quad (A.7)$$

$$dP_e/dt = \{P_m, P_e\} - \{P_e, K_e\} - P_{e_{dis}}. \quad (A.8)$$

From Eqs. (2.1)–(2.6) the following expressions can be derived (see Semtner and Mintz 1977; McWilliams et al. 1978; Bleck 1985):

$$\{K_m, K_e\}_a = \bar{u}(\overline{\nabla u' \cdot \mathbf{u}'} + \overline{w'u'_z}) + \bar{v}(\overline{\nabla v' \cdot \mathbf{u}'} + \overline{w'v'_z})h \quad (A.9a)$$

$$\{K_m, K_e\}_b = [\overline{up}_s(\overline{\nabla u' \cdot \mathbf{u}'} + \overline{s'u'_s}) + \overline{vp}_s(\overline{\nabla v' \cdot \mathbf{u}'} + \overline{s'v'_s})]/g \quad (A.9b)$$

$$\{K_m, K_e\}_c = -\bar{u}_y(\overline{u'v'})h \quad (A.9c)$$

$$\{P_m, P_e\}_a = agh\overline{T\nabla \cdot \mathbf{u}'T'}/\bar{T}_z \quad (A.10a)$$

$$\{P_m, P_e\}_b \text{ not defined} \quad (A.10b)$$

$$\{P_m, P_e\}_c = (\overline{\psi_2 - \psi_1})(\overline{u'_1v'_2 - u'_2v'_1})F_1h \quad (A.10c)$$

$$\{P_e, K_e\}_a = -ahg\overline{T'w'} \quad (A.11a)$$

$$\{P_e, K_e\}_b = (\overline{\Phi\nabla \cdot (\mathbf{u}'p_s)} - \overline{\mathbf{u}' \cdot p_s\nabla p}/\rho)/g \quad (A.11b)$$

$$\{P_e, K_e\}_c = (\partial/\partial t\overline{F_i(\psi_2 - \psi_1)'_i\psi'_i} - F_i\overline{\psi_i}(\overline{u'_1v'_2 - u'_2v'_1}))h(-1)^{i-1} \quad (A.11c)$$

$$\{K_m, P_m\} = agh\overline{Tw} \quad (A.12a)$$

$$\{K_m, P_m\} = (-\overline{\Phi\nabla \cdot (p_s\bar{\mathbf{u}})} + \bar{\mathbf{u}} \cdot \overline{p_s\nabla p}/\rho)/g \quad (A.12b)$$

$$\{K_m, P_m\} = (\partial/\partial t\overline{F_i(\psi_2 - \psi_1)_t\psi_i} + F_i\overline{\psi_i}(\overline{u'_1v'_2 - u'_2v'_1}))h(-1)^i \quad (A.12c)$$

In these equations Φ denotes the geopotential.

In the isopycnic model the $\{P_m, P_e\}$ is not defined (Bleck 1985), whereas in isopycnic coordinates the potential energy itself instead of the available potential energy can be partitioned into a P_e and a P_m term. The drawback is that $\{P_m, P_e\}$ vanishes.

REFERENCES

Arakawa, A., and V. R. Lamb, 1977: Computational design of the basic dynamical processes of the UCLA General Circulation Model. *Methods in Comput. Phys.*, **17**, 173–265.

Batchelor, G. K., 1953: *The Theory of Homogeneous Turbulence.* Cambridge University Press, 197 pp.

Bennet, A. F., and D. B. Haidvogel, 1983: Low-resolution numerical simulation of decaying two-dimensional turbulence. *J. Atmos. Sci.*, **40**, 738–748.

Bleck, R., 1985: On the conversion between mean and eddy components of potential and kinetic energy in isentropic and isopycnic coordinates. *Dyn. Atmos. Oceans*, **9**, 17–37.

——, and D. B. Boudra, 1981: Initial testing of a numerical ocean circulation model using a hybrid vertical coordinate. *J. Phys. Oceanogr.*, **11**, 755–770.

——, and ——, 1986: Wind driven spin-up in eddy-resolving ocean models formulated in isopycnic and isobaric coordinates. *J. Geophys. Res.*, **91**, 7611–7621.

Böning, C. W., 1989: Eddies in a primitive equation model: Sensitivity to horizontal resolution. *Ocean Modelling*, **85**, 3–5.

——, and M. D. Cox, 1988: Particle dispersion and mixing of conservative properties in an eddy-resolving model. *J. Phys. Oceanogr.*, **18**, 320–338.

Boris, J. P., and Book, D. L., 1973: Flux-corrected transport, I, SHASTA, a fluid transport algorithm that works. *J. Comput. Phys.*, **11**, 38–69.

Bryan, F., 1987: Parameter sensitivity of primitive equation ocean general circulation models. *J. Phys. Oceanogr.*, **17**, 970–985.

Bryan, K., 1969: A numerical method for the study of the circulation of the world ocean. *J. Comput. Phys.*, **4**, 347–376.

——, 1986: Poleward Buoyancy transport in the ocean and mesoscale eddies. *J. Phys. Oceanogr.*, **16**, 927–933.

Charney, J. G., 1971: Geostrophic turbulence. *J. Atmos. Sci.*, **28**, 1087–1095.

Cox, M. D., 1985: An eddy-resolving numerical model of the ventilated thermocline. *J. Phys. Oceanogr.*, **15**, 1312–1324.

——, 1987: Isopycnal diffusion in a *z*-coordinate ocean model. *Ocean Modelling*, **74**, 1–5.

Cummins, P. F., G. Holloway, and A. E. Gargett, 1990: Sensitivity of the GFDL ocean general circulation model to a parameterization of vertical diffusion. *J. Phys. Oceanogr.*, **20**, 817–830.

Drijfhout, S. S., 1990: Eddy-genesis and the related transports of heat, momentum and vorticity: A parameter study. *J. Phys. Oceanogr.*, **20**, 1645–1665.

Flierl, G. R., 1975: Gulf Stream meandering, ring formation and ring propagation. Ph.D. dissertation, Harvard University. 265 pp.

Fox, D. G., and S. A. Orszag, 1973: Inviscid dynamics of two-dimensional turbulence. *Phys. Fluids*, **2**, 169–171.

Gent, P. R., and J. C. McWilliams, 1990: Isopycnal mixing in ocean circulation models., *J. Phys. Oceanogr.*, **20**, 150–155.

Holland, W. R., 1978: The role of mesoscale eddies in the general circulation of the ocean—numerical experiments using a wind-driven quasigeostrophic model. *J. Phys. Oceanogr.*, **8**, 363–392.

——, and P. B. Rhines, 1980: An example of eddy-induced ocean circulation. *J. Phys. Oceanogr.*, **11**, 1010–1031.

——, and M. L. Batteen, 1986: The parameterization of subgrid-scale heat diffusion in eddy-resolved ocean circulation models. *J. Phys. Oceanogr.*, **16**, 200–206.

——, T. Keffer, and P. B. Rhines, 1984: Dynamics of the ocean general circulation: The potential vorticity field. *Nature*, **308**, 698–705.

Huang, R. X., and K. Bryan, 1987: A multilayer model of the thermohaline and wind-driven ocean circulation. *J. Phys. Oceanogr.*, **17**, 1909–1924.

Ikeda, M., 1981: Meanders and detached eddies of a strong eastward flowing jet using a two-layer quasigeostrophic model. *J. Phys. Oceanogr.*, **11**, 526–540.

——, and J. R. Apel, 1981: Mesoscale eddies detached from spatially growing meanders in an eastward flowing oceanic jet using a two-layer quasigeostrophic model. *J. Phys. Oceanogr.*, **11**, 1638–1661.

Iselin, C. O., 1939: The influence of vertical and lateral turbulence on the characteristics of the waters at mid-depths. *Eos, Trans., Amer. Geophys.* Union **20**, 414–417.

Kraichnan, R., 1967: Inertial ranges in two-dimensional turbulence. *Phys. Fluids*, **10**, 1417–1423.

Lorenz, E. N., 1955: Available potential energy and the maintenance of the general circulation. *Tellus*, **7**, 157–167.

McDougall, T. J., 1987: Neutral surfaces. *J. Phys. Oceanogr.*, **17**, 1950–1964.

——, and J. A. Church, 1986: Pitfalls with the numerical representation of isopycnal and diapycnal mixing. *J. Phys. Oceanogr.*, **16**, 196–199.

McWilliams, J. C., W. R. Holland, and J. H. S. Chow, 1978: A description of numerical Antarctic Circumpolar currents. *Dyn. Atmos. Oceans*, **2**, 213–291.

Monin, A. S., and R. V. Ozmidov, 1985: *Turbulence in the Ocean.* Reidel, 247 pp.

Montgomery, R. B., 1940: The present evidence on the importance

of lateral mixing processes in the ocean. *Bull. Amer. Meteor. Soc.*, **21**, 87–94.

Pratt, L. J., and M. E. Stern, 1986: Dynamics of potential vorticity fronts and eddy detachment. *J. Phys. Oceanogr.*, **16**, 1101–1120.

Redi, M. H., 1982: Oceanic isopycnal mixing by coordinate rotation. *J. Phys. Oceanogr.*, **12**, 1154–1158.

Rhines, P. B., 1976: The dynamics of unsteady currents. *The Sea, Vol. 6, Marine Modeling*, E. D. Goldberg, I. N. McCave, J. J. O'Brien, and, J. H. Steele, Eds., Wiley-Interscience, 189–318.

Robinson, A. R., 1983: *Eddies in Marine Science*. Springer-Verlag, 609 pp.

——, J. R. Luyten, and F. C. Fuglister, 1974: Transient Gulf Stream meandering. Part I: An observational experiment. *J. Phys. Oceanogr.*, **4**, 237–255.

——, D. E. Harrison, Y. Mintz, and A. J. Semtner, 1977: Eddies and the general circulation of an idealized oceanic gyre: A wind and thermally driven primitive equation numerical experiment. *J. Phys. Oceanogr.*, **7**, 182–207.

——, M. A. Spall, and N. Pinardi, 1988: Gulf Stream simulations and the dynamics of ring and meander processes. *J. Phys. Oceanogr.*, **18**, 1811–1853.

Semtner, A. J., and Y. Mintz, 1977: Numerical simulation of the Gulf Stream and midocean eddies. *J. Phys. Oceanogr.*, **7**, 208–230.

——, and W. R. Holland, 1978: Intercomparison of quasigeostrophic simulations of the western North Atlantic circulation with primitive equation results. *J. Phys. Oceanogr.*, **8**, 735–754.

Spall, M. A., and A. R. Robinson, 1990: Regional primitive equation studies of the Gulf Stream meander and ring formation region. *J. Phys. Oceanogr.*, **20**, 985–1016.

Zalesak, S. T., 1979: Fully multidimensional flux-corrected transport algorithms for fluids. *J. Comput. Phys.*, **31**, 335–362.